Ge Nanocages and Nanoparticles Via Microwave-assisted Galvanic Replacement for Energy Storage Applications

Xiao Qi[1] and Susan M. Kauzlarich [*,1]

[1]Department of Chemistry, University of California, One Shields Avenue, Davis, California 95616, United States

Abstract

We report a systematic study on the synthesis of highly monodisperse hollow Ge nanoparticles via galvanic replacement reactions between GeI_2 and Ag NPs. By fine-tuning the synthetic parameters such as temperature, precursor molar ratio, ligand concentration, etc., the morphology and surface structure of the Ge NPs can be precisely controlled. We also report a method to synthesize solid Ge NPs and Ag@Ge core-shell metal-semiconductor NPs with controllable uniform shell thickness. An inward diffusion mechanism for galvanic replacement is proposed and supported by imaging the different stages of the reaction and analysis of the products. This mechanism allows the reaction to be self-terminated and achieve nanometer-sized accuracy. The galvanic reaction may be applied to other semiconductors and could serve as a powerful alternative to the classical nucleation-growth mechanism and subsequently advance the scale up and further energy storage applications.

KEYWORDS: *germanium nanoparticles, galvanic replacement reaction, hollow nanoparticles, core-shell structure, colloidal synthesis, inward and outward diffusion, nanocages*

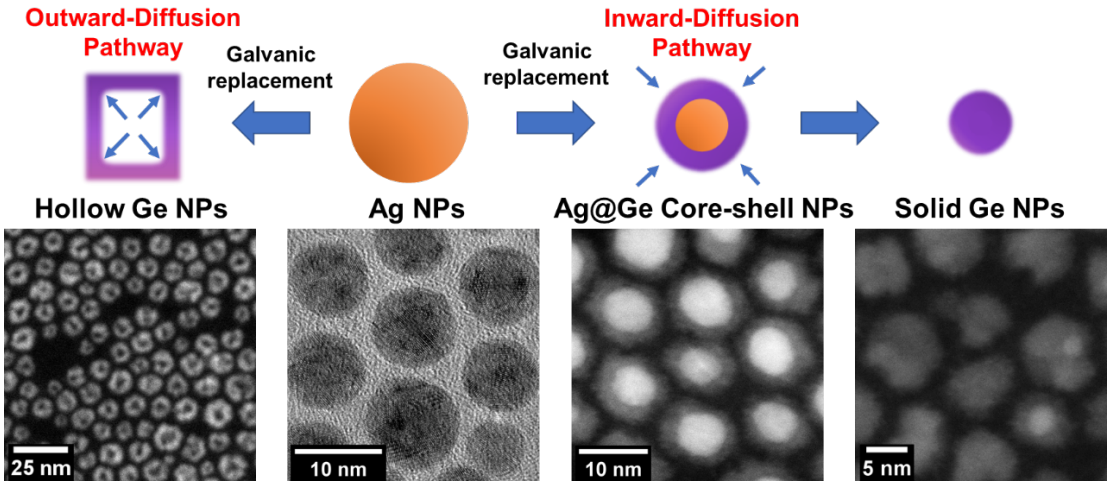

1. Introduction

The search for high energy density electrode materials is prompted by the large market demand for new energy-storage devices and electric vehicles (EVs) worldwide.[1-5] The substantial increase in charge capacity of battery particularly relies on the improvement of the anode materials.[6] Nanostructured germanium (Ge) is one of the most promising candidates for the next generation anode materials for lithium ion battery (LIB) applications owing to its high Li storage densities and high lithium ion diffusivity and conductivity.[7-9] Due to the low cost and flexibility of solution-based processing techniques such as spin-coating, spray-coating, inkjet and screen printing, many efforts have been made aiming to develop colloidal synthetic methods for the preparation of Ge nanoparticles (NPs). Although progress was being made over the last decade,[10] less success on morphology and size control of colloidal Ge NPs has been achieved. Compared to the ubiquitous II-VI, III-V, IV-VI semiconductor and noble metal nanocrystals, well-defined shapes are more difficult to achieve for Ge nanomaterial synthesis due to the strong covalent nature of Ge-Ge bonds. Thus, common strategies such as thermal decomposition or reduction of organogermane precursors usually lead to unstable products.[11, 12] Therefore, a facile and versatile synthesis route to shape directed Ge nanostructures is highly desirable and a thorough understanding of the reaction mechanism is vital for further scale-up and energy storage applications..

In addition to the conventional synthetic strategies, a galvanic replacement reaction provides a simple and versatile route for reducing noble metal precursor and generating nanostructures with controllable pores and compositions. During the past two decades, many elegant and remarkable syntheses have been performed by cooperative galvanic replacement reactions and have produced a variety of nanoscale structures with complex morphologies.[13-17] Most of the research work was based on the transformation of noble metal such as Au, Pd, and Pt due to their robustness. For example, the reaction mechanism between single crystal silver nanocubes and chloroauric acid have been studied by many groups.[18-23] However, synthesis of semiconductor nanostructure via galvanic replacement reaction has been rarely reported and not well studied. Most of the successful galvanic replacement reactions were performed in aqueous solution, typically possess a very low energy barrier, and can be easily triggered at room or lower temperatures. This is not the case for semiconductor materials due to their strong covalent bonding nature, plus they can be air and water sensitive which means the reaction can only be performed under a nonaqueous and air-free environment. In addition, due to the lack of understanding of such mechanism, it's hard to find a suitable binding ligand to not only stabilize the template particles and products but also to facilitate the replacement reaction under moderate synthesis condition. We demonstrated the unconventional transformation of inorganic germanium precursors (e.g., GeI_2) to hollow Ge NPs through galvanic replacement with

Ag NPs.[24] In this reaction, Ge^{2+} oxidizes Ag to Ag^{+}, which causes the hollowing-out of the sacrificial Ag NP templates. However, the details of the mechanism have remained largely unknown due to the complexity of the reaction system. For example, unlike the conventional galvanic replacement reaction between noble metals, the large lattice mismatch between Ag and Ge (38.7%) would prevent the formation of alloy nanostructures, which is a common intermediate product for such replacement reaction, thus a new reaction mechanism needs to be proposed. What's more, the specific roles of each reagent in the galvanic replacement between GeI_2 and Ag nanoparticles need to be understood in order to help develop an efficient and highly reproducible process for producing hollow Ge NPs with high yield and desirable qualities (e.g. narrow size distribution, well-defined morphology, etc.). The Scheme provides a schematic as to the synthetic route and impact of the parameters investigated. The better understanding of the reaction mechanism and the interaction of the various components to the structural evolution provides vital information for scale-up and industrial applications.

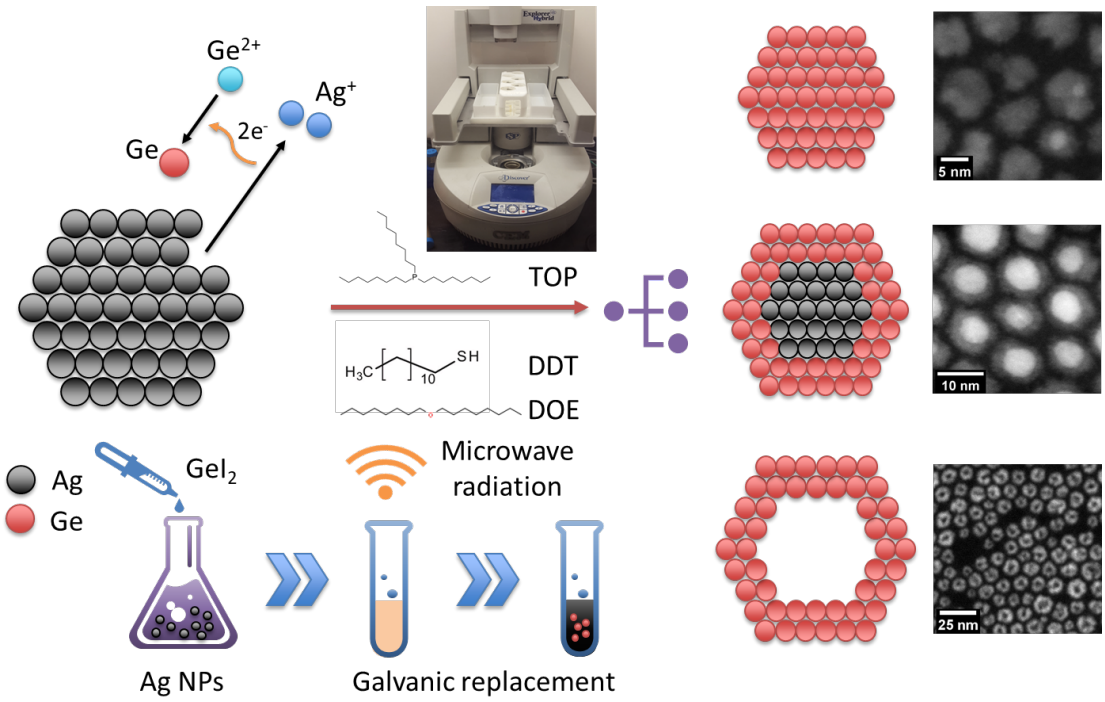

Scheme 1. Microwave reaction of GeI_2 with Ag nanoparticles and the impact of various organic reagents on the shape and composition of the final product.

2. Experimental Section

Chemicals and Materials. Silver(I) nitrate, $AgNO_3$ (≥99.0%, Sigma-Aldrich), was used as received. Phase pure germanium (II) iodide, GeI_2, was purchased from Prof. Richard

Blair's laboratory (University of South Florida). Oleylamine, OAm (>40%, TCI America), dioctyl ether, DOE (99%, Sigma-Aldrich), dodecanethiol DDT (98%, Sigma-Aldrich) were degassed at 100 °C under argon flow for 1h prior to use. Tri-n-octylphosphine, TOP (min. 97%, Strem Chemicals), was used as received. Methanol and toluene were purchased from Fisher Scientific, purified using a solvent purification system, degassed, and stored under inert atmosphere conditions in an argon-filled glovebox.

Synthesis of Silver Nanoparticles. In an argon-filled glovebox, 5 mmol of $AgNO_3$ was added to 50 mL of OAm in a two-neck round-bottom flask equipped with a stopcock adapter and rubber septum. The flask was connected to a Schlenk line, and the suspension was then heated up to 60 °C. The temperature was maintained until the granular $AgNO_3$ crystals are completely dissolved. The solution was then quickly heated with a ramp ≥ 10 °C min^{-1} to 200 °C for 40 min while under an argon flow. The reaction was initially colorless, but as the $AgNO_3$ was reduced to form OAm stabilized Ag NPs, the reaction turned dark brown. Upon cooling to room temperature, the Ag NPs were isolated using a toluene/methanol system under argon protection. The mixture was centrifuged at 8500 rpm for 10 min. The supernatant was discarded and the precipitates were re-dispersed in toluene for further characterization. To prepare the galvanic replacement reaction between Ag and GeI_2, the Ag NPs precipitates were directly pumped in the glovebox and re-dispersed in DOE for further use. Unless otherwise stated, the Ag NPs used for the following galvanic replacement reaction come from same reaction batch in order to ensure their uniformity.

Controlled Synthesis of Ge NPs and Ag/Ge Core-shell Intermediates. In a typical synthesis, under inert atmosphere conditions, 0.25 mmol GeI_2 was sonicated in 4.2 mmol TOP until it became a uniform yellowish solution. About 0.5 mmol Ag NPs dispersed in 20.78 mmol of DOE was transferred to a 35 mL microwave vessel followed by addition of the GeI_2/TOP solution and 5 mmol of DDT. The microwave vessel was sealed with a silicone cap purchased from CEM, transferred to a CEM microwave reactor (Discover SP) and heated to 200 °C in dynamic mode. After heating 30 min at 200°C, the reaction was cooled to 60 °C in the reactor chamber by air blowing and then completed quenched in an ice-water bath. The microwave vessel was covered by parafilm and pump into a glove box. The resulting product was washed with toluene/methanol and centrifuged at 8500 rpm for 10 min three times. The supernatant was discarded each time, and the Ge NPs were dispersed in toluene and stored in a glass vial within the glovebox. For the synthesis details of all the reactions of this systematic study, see supporting information (SI, Table S1).

Characterization

High-angle annular dark field scanning TEM (HAADF-STEM) images of the sample were obtained by using an aberration-corrected JEOL JEM-2100F/Cs STEM operated at 200 kV. The sample was prepared by putting one droplet of toluene dispersions of the as synthesized NPs on copper grids coated with ultrathin amorphous carbon films (Ted Pella,

Inc.). Energy-dispersive X-ray spectroscopy (EDS) were collected on an Oxford X-MaxN TSR EDS detector attached to the JEOL JEM-2100F to investigate the chemical composition and structural information. TEM data were acquired using a FEI ThemIS 60−300 STEM/TEM (Thermo Fisher Scientific, US) operated at 300 kV at the National Center for Electron Microscopy within the Molecular Foundry in Lawrence Berkeley National Laboratory. The ThemIS is equipped with image aberration corrector optics, and a Ceta2 camera (4k × 4k pixels, and 14-bit dynamic range). EDS mapping was performed using a Bruker Super-X Quad windowless detector with a solid angle of 0.7 sr. The measurement of optical property was conducted on the toluene dispersion with a Shimadzu UV-3600.

3. Results and Discussion

3.1 Synthesis of Ag NPs

In order to synthesize Ge NPs through a galvanic replacement reaction, spherical Ag NPs as the sacrificial template are first prepared. GeI_2 is directly reduced by Ag and deposited onto the surface of the Ag NPs, thus monodispersity of the Ag NPs is critical for the morphology control of the final products as well as solubility in an organic solvent. A one-step synthesis of Ag NPs in an organic solvent was performed by optimizing a previously reported procedure.[25-27] The Ag NPs (shown in Figure 1) were stabilized by OAm ligands and remain stable in air for several days. Characterization by TEM showed that the Ag NPs are spherical and have a narrow size-distribution (9.51 ± 0.62 nm). Lattice fringes indicate that the Ag NPs are polycrystalline. The UV-vis spectrum displayed the expected surface plasmon resonance band with an absorbance maximum at 421 nm.[25, 26]

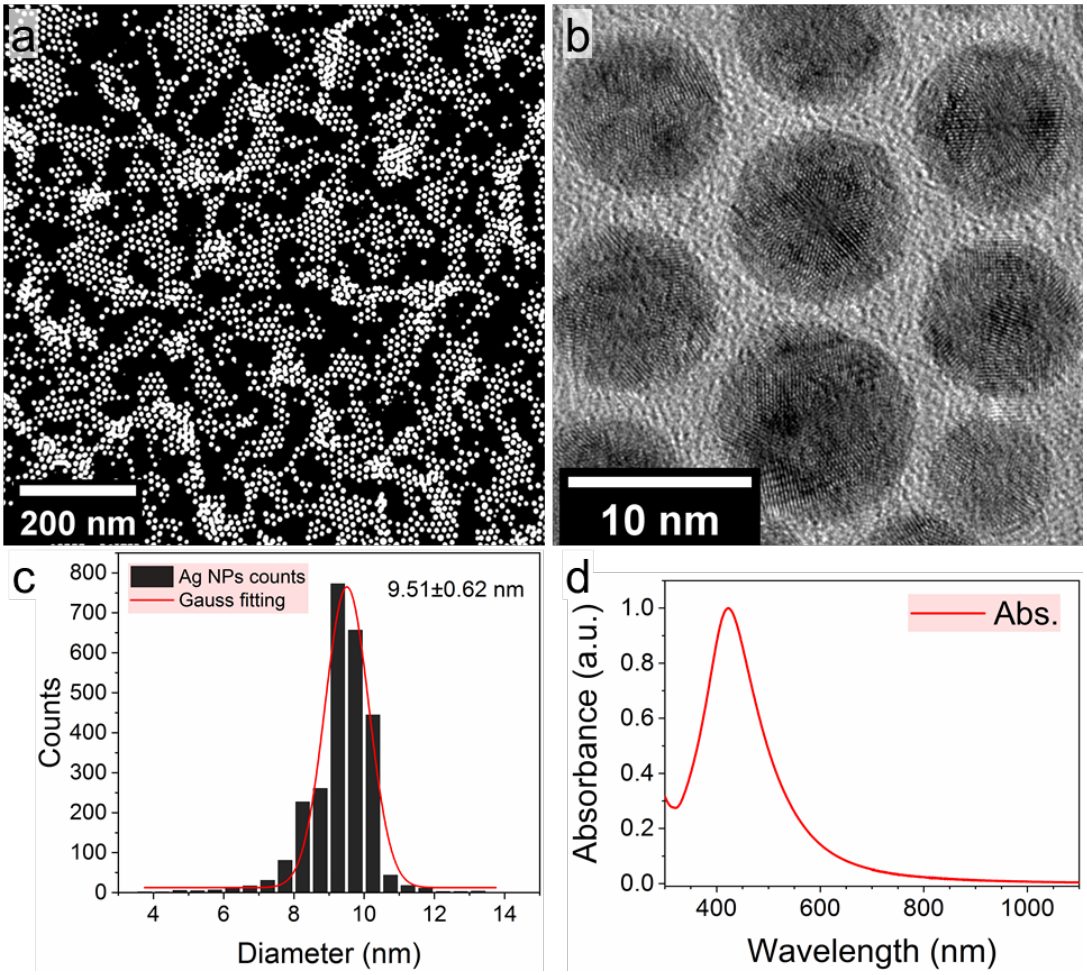

Figure 1. (a) Dark-field STEM image of as-synthesized spherical, oleylamine-stabilized Ag NPs. (b) Bright-field HRTEM image of the Ag NPs. (c) Histogram data of the size distribution from (a). An average size of 9.51 nm and a standard deviation about 0.62 nm were calculated from Gaussian fitting to the histogram. (d) UV-vis spectrum of Ag NPs in toluene. The surface plasmon resonance (SPR) shows a maximum at 421 nm.

3.2 Synthesis of Ge NPs

Ge NPs are synthesized under elevated temperature via galvanic replacement by employing Ag NPs as the sacrificial template with DOE as an aprotic solvent and TOP and DDT as the co-surfactants. The anisotropic growth and structural evolution during galvanic replacement are systematically investigated by using ex situ methods after systematically adjusting the synthetic parameters. The results provide insight into the mechanism and the roles of each component on the final products.

3.2.1 The role of TOP

To investigate the role of TOP, the amount of TOP was gradually increased while keeping all other reaction parameters the same. The Ag/Ge molar ratio was kept as 2:1 which is the exact stoichiometric relationship according to the galvanic replacement reaction: $2Ag + GeI_2 \rightarrow Ge + 2AgI$. In this synthesis, GeI_2 is first added to TOP and sonicating for 10 min, a clear yellowish solution appears which indicates GeI_2 is completely dissolved. When the molar ratio between TOP and Ge is increased from 8:1 to 16:1 and finally to 32:1, hollow Ge NPs were produced exclusively in all cases as seen in the HAADF-STEM images in Figure 2a-f; EDS spectrum is shown in supporting information (SI, Figure S2).The hollow Ge NPs are totally Ag-free, indicating complete galvanic replacement. The high magnification images in Figure 2 show that hollow Ge NPs synthesized with lower TOP content results in a bumpy and rough surface, while higher TOP content result in hollow Ge NPs that are smoother on the surface. This result could be explained by the influence of TOP concentration on the mobility of Ge^{2+} and AgI in the solution. We propose that the higher concentration of TOP decreases the affinity of Ge^{2+} to the Ag NPs surface thus lower the deposition rate of Ge atoms, which allows the Ge atoms sufficient time to migrate to the particle surface. The slower rate of deposition and atom/ion mobility would eventually reduce the dangling bonds, lower the overall surface energy and thus increase the smoothness of the hollow Ge NPs. On the other hand, TOP is also served as an important solvent to dissolve GeI_2. As GeI_2 does not dissolve in DOE, our attempt to synthesis the Ge NPs without TOP failed due to the solubility issue. By adding GeI_2 directly into the microwave vessel which preloaded with Ag NPs, DOE and DDT and heating at 200 °C for 30 min, no Ge NPs are obtained and GeI_2 powder is still present as a sediment at the bottom of the microwave tube.

While this surface shape-directing effect of TOP is rarely found in the literature, similar results were reported by Xia and coworkers when they compared the galvanic replacement between Ag nanocubes and Pd^{2+} or Pt^{2+} ions in aqueous solution.[28] While the reaction of Ag nanocubes with Na_2PdCl_4 resulted in the formation of smooth Pd-Ag nanoboxes, Pt nanoboxes with bumpy surfaces were formed if Na_2PdCl_4 was replaced by Na_2PtCl_4. It is well known that alloying is the basis for retaining the morphology of the original template during a galvanic replacement reaction.[16] In their case, the Pt and Ag cannot form a homogenous alloy at the synthesis temperature (100 °C) due to the high bonding energy of Pt-Pt, which lead to the continuous nucleation and growth of Pt on the Ag nanocubes surface and form an amorphous rough layer on the Ag nanocubes.

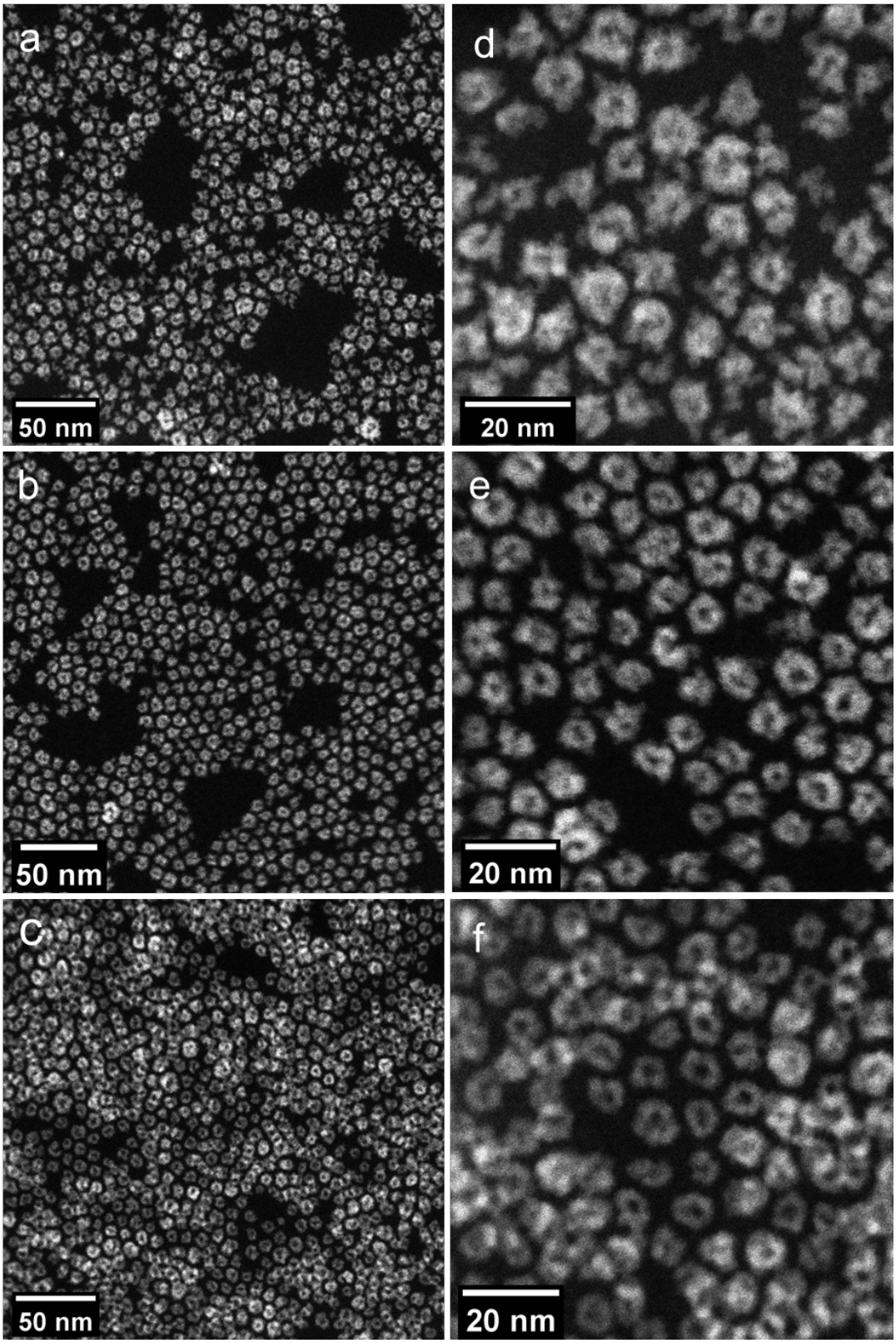

Figure 2. (a-c) HAADF-STEM images of hollow Ge NPs synthesized from the same

batch of Ag NPs via galvanic replacement reaction. The TOP/Ge molar ratio are (a) 8:1, (b) 16:1, (c) 32:1. Scale bar are all 50 nm. (d) High magnification image from (a), the surface of the hollow Ge NPs is bumpy and rough. (e) High magnification image from (b), the Ge NPs are smoother than in (d). (f) High magnification image from (c), the as-synthesized Ge NPs have a very smoothly surface with well-defined interior.

3.2.2 The role of DDT

DDT is a common L-type capping ligand which contains an electron-rich thiol group and behaves as a Lewis base which coordinates to the electron-poor Lewis acid-like metal or semiconductor nanoparticles.[47] This coordination passivates the dangling bonds at the surface, and the long alkane chain helps to prevent further growth or agglomeration through van der Waals forces.[29] This strategy usually benefits from having the capping molecule in large excess which helps to efficiently protect the particle surface without changing the particle shape. However, our study shows that the excess amount of DDT can also change the morphology feature of the final products and generate porous Ge nanocages. By simply increasing the concentration of the capping ligand, DDT, while keeping the Ge^{2+} ion concentration constant, more vacancies are generated on the surface of the particles which leads to the formation of more complex Ge nanocages and nanoframes.

To understand the role of DDT in the synthesis, the molar ratio of DDT/Ag was changed from 4 to 20 while keep all other parameters constant. As the HAADF-STEM images show in Figure 3, when the molar ratio of DDT/Ag equals to 4, uniform hollow Ge NPs were synthesized with a small number of larger particles, which are present as the brighter particles in the HAADF-STEM image. However, when the molar ratio between DDT and Ag NPs was increased to 8, the amount of larger and thicker hollow Ge NPs was significantly increased. Figure 3e clearly shows the nanoframes morphology and multiple porous walls. This trend continues with DDT and Ag NPs molar ratio of 12, as Figure 3f shows that the nanocages became a dominant morphology of the overall particles. However, when the molar ratio between DDT and Ag NPs was further increased to 16 and even 20, the yield of hollow Ge NPs dramatically decreases, resulting in an amber/orange color solution which may be due to dissolving and the collapse of the nanocage structure. These results indicate the important role of DDT in the geometry evolution of the nanocage formation process. Similar to the discussion on the role of TOP, regardless of the DDT/Ag molar ratio, the resulting hollow Ge NPs are all Ag content free, which suggests that all the Ag NPs are completely oxidized to Ag^{+} and removed with the isolation process. (EDS spectrum is shown in SI, Figure S3)

Previous studies show that the formation of nanocages with multiple porous walls are involved with the dealloying process of a bi-metallic system.[16, 19, 30, 31] The dealloying can be achieved either by increasing the metal ion concentration or by utilizing a selective

etchant to remove the metal template.[19, 30] In the galvanic replacement reaction between Ag NPs and GeI_2, DDT can act as a selective etchant which facilitates the extracting of Ag atoms through a S-Ag coordination bond. When the concentration of DDT is lower, the direct contact between Ag atoms and Ge^{2+} ions are limited to the surface of the Ag NPs due to the immobility of the inner Ag atoms. The formation of a thin and incomplete layer of Ge on the surface can prevent the inner Ag atoms from reacting with Ge^{2+}. As a result, the small hole serves as the primary site for continuous diffusion of Ge^{2+} which leads to the formation of small Ge NPs with a single pinhole. While under higher concentration, DDT can facilitate the fast removal of Ag atoms which can subsequently increase the pore size and expansion rate of the Ge NPs and resulting in the formation of larger porous Ge nanocages.

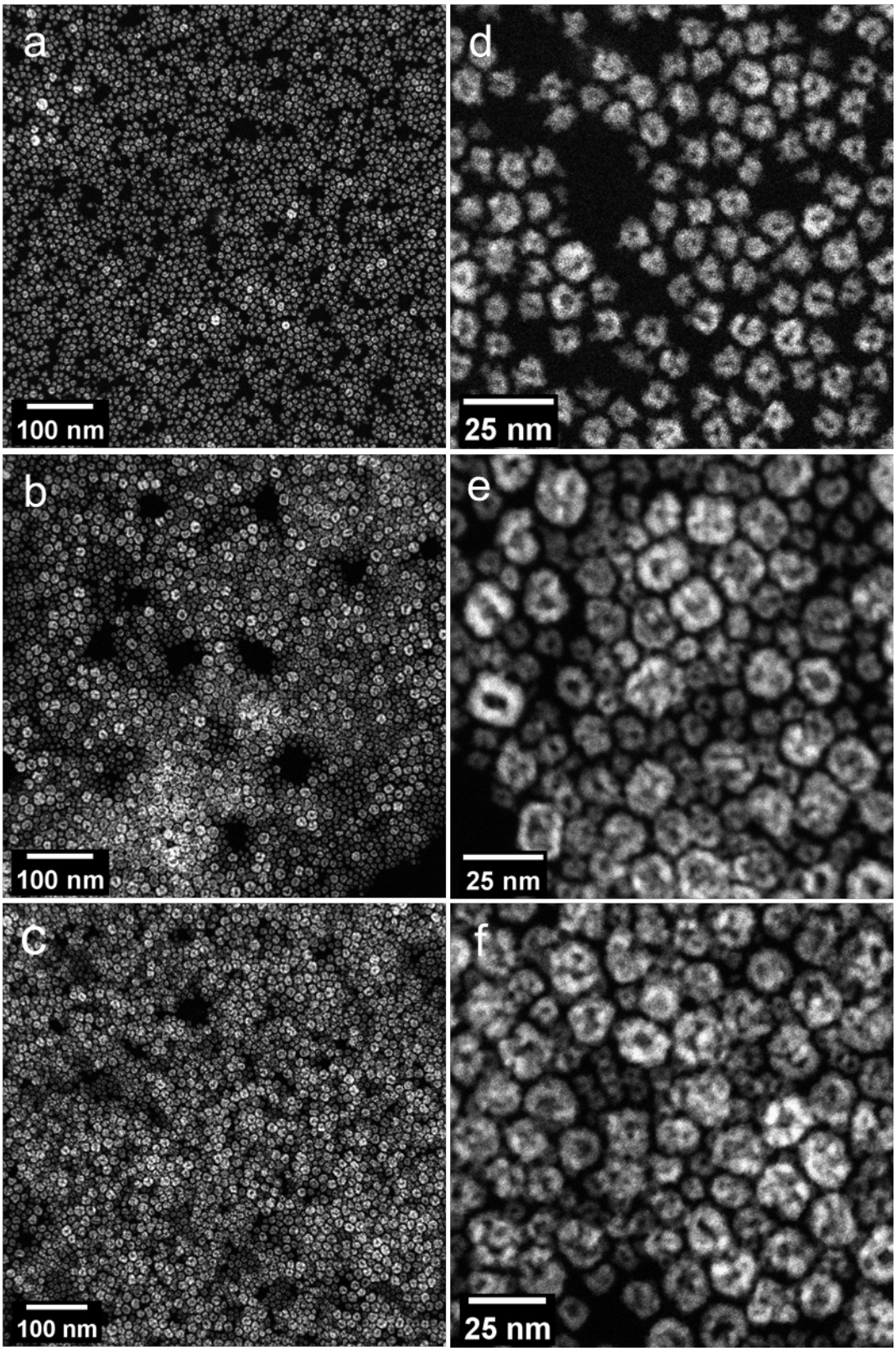

Figure 3. (a) HAADF-STEM images of hollow Ge NPs synthesized from the same batch of Ag NPs via galvanic replacement reaction with the variation of DDT/Ag

molar ratio of (a) 4:1, (b) 8:1, (c) 12:1. Scale bar are all 100 nm. (d) High magnification image from (a), the as-synthesized hollow Ge NPs have very uniform size and thickness. (e) High magnification image from (b), the Ge NPs are polydisperse in terms of both size and thickness. Some of the particles are apparently larger and show nanocage structure (f) High magnification image from (c), the image shows a majority of more complex nanocage structure with a larger size.

3.2.3 Ge/Ag ratio influence

The GeI_2/Ag NPs molar ratio was gradually decreased from 0.8 to 0.1, while keeping all other parameters the same. While increasing the GeI_2/Ag ratio higher than the stoichiometric ratio does not affect the quality of hollow Ge NPs, as shown in Figure 4a (GeI_2/Ag ratio = 0.8) and 4b (GeI_2/Ag ratio = 0.6); decreasing the GeI_2 content below the stoichiometric ratio does significantly change the final products. When the molar ratio of GeI_2/Ag was further lower to 0.4, as shown in Figure 4c, a mixture of hollow Ge NPs and solid Ge NPs co-exist. When the molar ratio was further decreased to 0.3, as indicated in Figure 4d, the products mainly composed of a highly monodisperse amorphous Ge NPs with no holes. A low magnification image shown in Figure 4e indicates the uniform size distribution of the solid Ge NPs sample synthesized from a GeI_2/Ag ratio of 0.3. Small amount of unreacted Ag contents is also shown with a brighter intensity in the HADDF-STEM image due to the much higher atomic number of Ag (Z-contrast images). The accompanying EDS spectrum and elemental mapping shown in Figure 4g-i confirmed the existence of a small amount of unreacted Ag, due to the slight excess of Ag content. This indicates the reaction did not follow the fast hollowing-out pathway described above even at high temperature (T = 200°C). Therefore, the formation of solid Ge NPs must be through some other mechanism which is controlled by the molar ratio between the GeI_2 precursor and Ag NPs. On the other hand, further lowering of the GeI_2/Ag ratio lead to the formation of irregular Ge nanoparticles (GeI_2/Ag ratio = 0.2) and Ge nanorods (GeI_2/Ag ratio = 0.1), in those cases, agglomeration of excess Ag NPs were also found, as shown in SI, Figure S4.

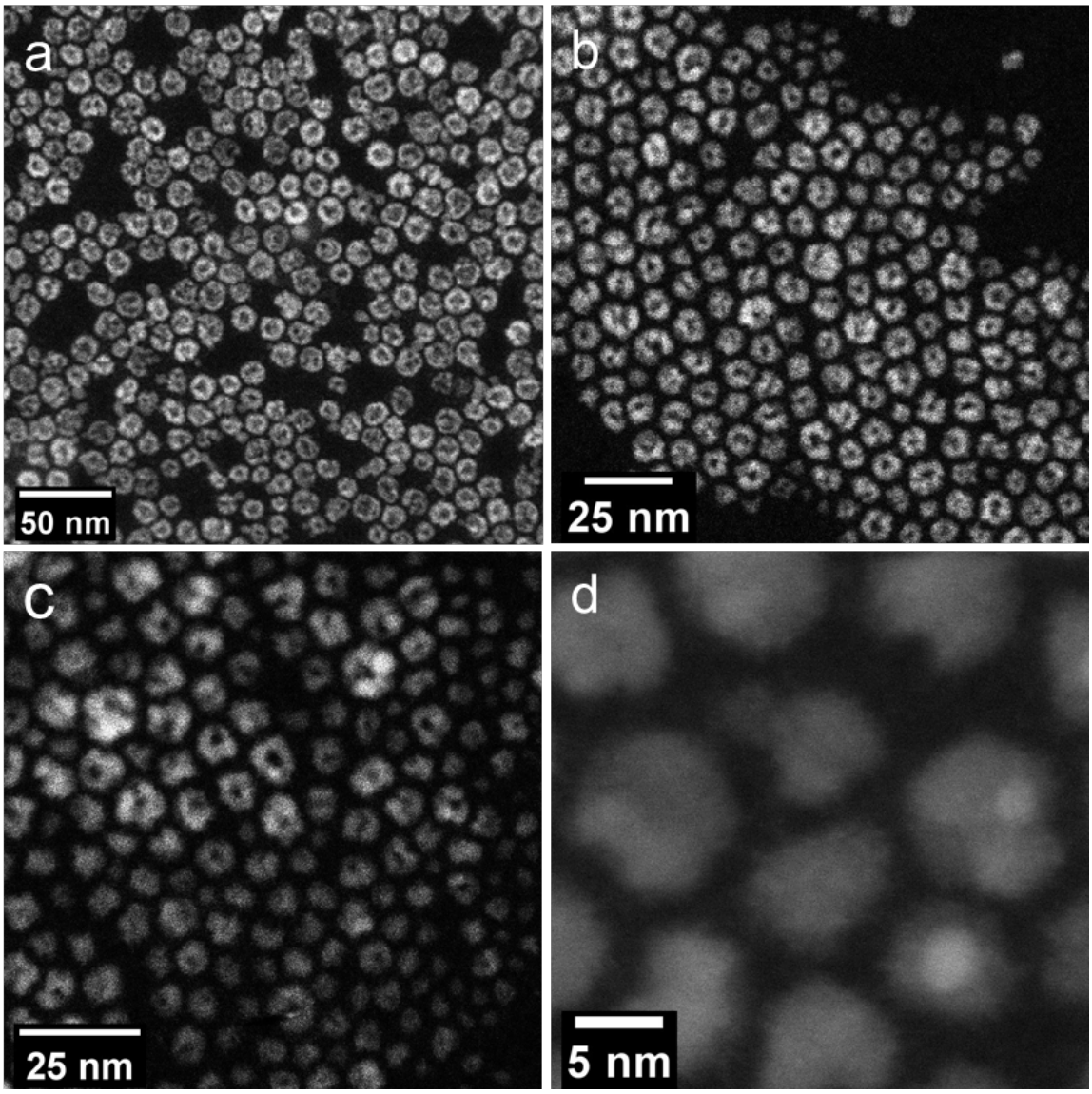
a
50 nm
b
25 nm
c
25 nm
d
5 nm

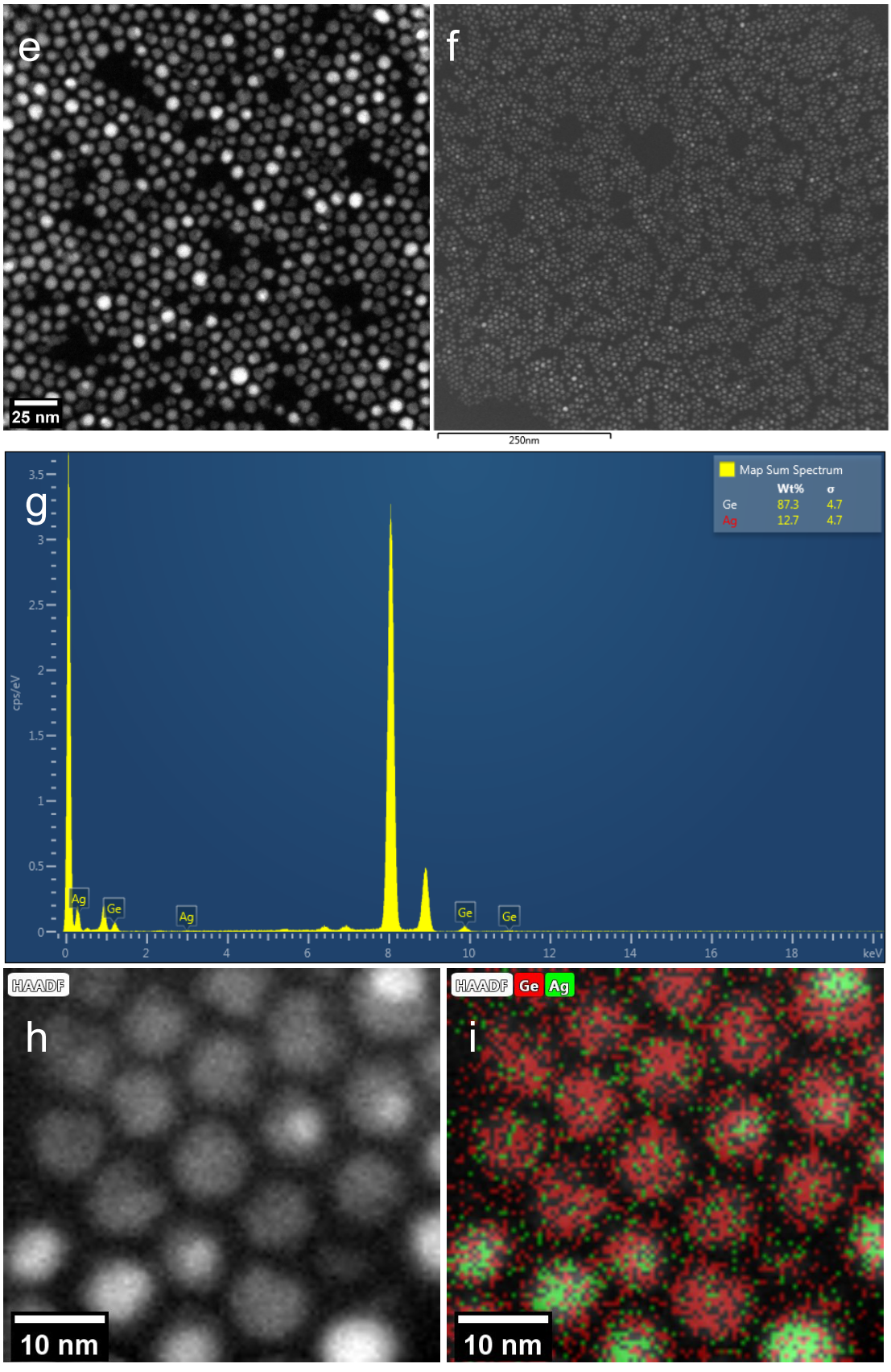
e
25 nm
f
250nm
g
Map Sum Spectrum
Wt% σ
Ge 87.3 4.7
Ag 12.7 4.7
cps/eV
keV
Ag
Ge
Ag
Ge
Ge
HAADF
h
10 nm
HAADF Ge Ag
i
10 nm

Figure 4. (a-d) HAADF-STEM images of Ge NPs synthesized from the same batch of Ag NPs via galvanic replacement reaction with the variation of GeI_2/Ag molar ratio of (a) 0.8, (b) 0.6, (c) 0.4, (d) 0.3. (e) A low magnification image from sample in 4d. (f) EDS survey image from sample in 4e. (g) EDS spectrum taken from the whole area in Figure 4f. (h-i) HAADF-STEM images from Figure 4e and EDS mapping confirmed that the bright spots are attributed to unreacted Ag.

In order to further understand the reaction mechanism, the molar ratio of GeI_2/Ag was held constant at 0.3 while decreasing the reaction time to 10 min and quenching the reaction in an ice-water bath. Figure 5 (a, b) represent the resulting bright field (BF) and dark field (DF) STEM image which show the expected Ag@Ge core-shell intermediate structure. From the BF-STEM image, we can clearly see the lattice fringes from the Ag core which indicates the original polycrystallinity feature of the Ag NPs. From the HAADF-STEM image, the different stages of the galvanic replacement reaction can be easily identified by marking a single particle with red dash circle. Site #1 shows the unreacted Ag NP and site #2 shows an Ag-Ge dimer which indicates the Ag NP was partially reduced by the Ge precursor which deposits the Ge atoms onto the adjacent domain. Site #3 indicate an Ag@Ge core-shell structure at a later stage of the replacement reaction. The Ag core shrinks to a very small size indicates that the Ag NP is almost fully reduced by the Ge precursor. Notice that there is no obvious void space formed between the Ag core and Ge shell. Site #4 represent a pure Ge NP without any Ag content. Corresponding EDS spectrum shown in Figure 5c reveal a much lower Ge/Ag ratio in the sample compared to Figure 4g, which indicates that an intermediate product is formed by shortening the reaction time.

With all the above information, we can propose a reaction mechanism to form completely amorphous solid Ge NPs. At an early stage, with significantly lower concentration of Ag NPs (0.3 vs. 0.5, which is the stoichiometric molar ration between GeI_2 and Ag), a thin layer of amorphous Ge is first deposited on the surface of the Ag NP without formation of any pinholes. So, the further galvanic replacement is happening under the interdiffusion through the thin Ge atomic layer. Due to the high lattice mismatch between the Ag and Ge and the larger size of Ag^+ compared to Ge^{2+}, along with the low concentration of Ag content, the inter-diffusion rate of Ge^{2+} is faster than the outer-diffusion rate of Ag^+, thus the reduced Ge atoms will occupy mainly the inner space of the particle. However, because of the stoichiometric relationship between the Ag and Ge^{2+}, more Ag atoms are oxidized than Ge atoms reduced and the overall size of the particle will continue shrink until all the Ag core been oxidized, leave a solid Ge NP as the final product. This hypothesis also explains the average size of the solid Ge NPs being smaller than the original Ag template.

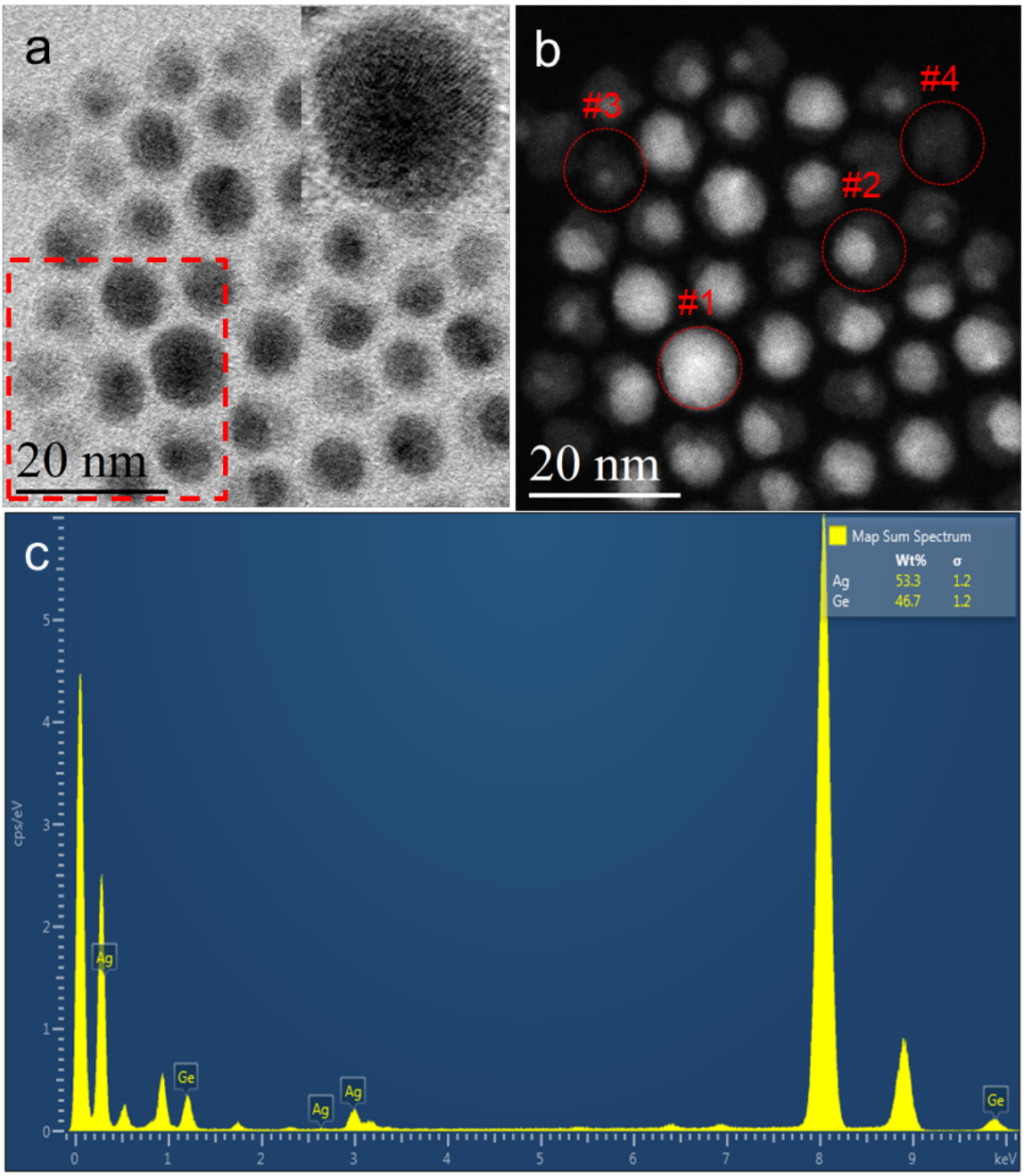

Figure 5. (a) BF-STEM image of the as-synthesized Ge NPs according to a GeI_2/Ag molar ratio equal to 0.3. The reaction was quenched after 10min with an ice-water bath and washed 3 times. The image shows a mixture of Ag NPs, solid Ge NPs and Ag@Ge core-shell NPs with different Ge thickness. Top-right corner insert shows a HR-STEM image of (a), the unreacted silver is highly polycrystalline. (b) Corresponding HAADF-STEM image of (a), elemental composition can easily be distinguished by the brightness due to the difference in z-contrast. The darker spot consist of Ge and much brighter spots are Ag. Particles at different stages of formation are marked with red dash circles. Site #1 shows unreacted Ag NP and

Site #2 shows an Ag/Ge dimer structure. Site #3 shows an Ag@Ge core-shell structure with small Ag core and Site #4 shows a pure solid Ge NP. (c) EDS spectrum taken from the whole area in Figure 5b.

In a typical galvanic replacement reaction, an internal void space will be generated in the final products. This can be explained from both stoichiometric and geometric arguments. First, as the metal ions in the solution phase have been reduced at the surface of the sacrificial template and are growing outward, the metal will be oxidized and extracted from the inner core. This process generates small holes and vacancies in the resulting nanostructures. In addition, the void size also depends on the stoichiometric ratio between the metal ions and the sacrificial template. For example, Xia et al,[32] did a comparative study of galvanic replacement reactions involving Ag nanocubes and $(AuCl_2)^-$ or $(AuCl_4)^-$. By substituting the gold precursor from $(AuCl_4)^-$ to $(AuCl_2)^-$, the stoichiometry between Ag and gold is changed owing to the difference in oxidation sate of the gold. The author reported both Au precursor can form hollow nanostructures, however, the vacancy space formed at different rate and only in case of $(AuCl_4)^-$, does the pinhole last throughout the reaction. In the example of $(AuCl_2)^-$, every Ag exchanges one Au atom, however; in the case of $(AuCl_4)^-$, every 3 Ag atoms need to be oxidized to generate enough electrons to reduce the Au ion. This difference in electrochemical reaction impacts the alloying/dealloying processes. Generally, with a higher oxidation state, a larger void space will be generated due to the faster extraction of the metal template. In our reaction, the deposition of each Ge atom would need to consume 2 Ag atoms inside, which helps the formation of inner void space. Thus, it's reasonable to assume that the hollowing-out process is dominated by the nanoscale Kirkendall effect, which arises from the difference of interdiffusion rate between two materials.[33]

Tang et al. reported the formation of Ag_2Se hollow nanocrystals through the reaction of selenium with both single crystalline (SC) and multiply twinned (MT) Ag NP.[34] Their study shows that, by contacting with selenium on the surface, the single-crystal Ag NP transform to Ag_2Se hollow nanocrystals through Kirkendall effect while the multiply twinned Ag NP give solid, homogeneous Ag_2Se nanocrystals. The author reasoned that, the diffusion of silver atoms is faster than that of selenium atoms, which lead to the void space formation and further condensed into a single hole. However, the multiple twinned structure can provide another fast atom diffusion path through the twining boundaries for both silver and selenium atoms, thus creating solid, homogeneous Ag_2Se nanocrystals. A similar explanation concerning the formation of solid amorphous Ge NPs is highly likely. Since the Ag template was unambiguously multiply twinned structure, it could provide an extra diffusion path through the defects thus counter-balancing the stoichiometric relationship between the Ag and Ge^{2+}, which implies a lower diffusion rate of Ag^+ and higher diffusion rate of Ge^{2+}. The overall reaction would deposit Ge inward towards to the core instead of outwards, leading to the formation of solid Ge NPs. The systematic study of the GeI_2/Ag

ratio influence also indicates that there is a threshold at around 0.3 where exclusively solid Ge NPs are formed.

The resulting solid Ge NPs are highly monodisperse owing to the uniform Ag NPs template and the unique reaction pathway. As shown in Figure 6, repeating the synthesis under similar condition but with longer reaction time results in a highly monodisperse Ge NP sample which shows the reaction is highly reproducible. By counting a total number of 1958 Ge NPs, the particles mean diameter is around 5.17 nm with less than 0.2% discrepancy between the two different fields of view and a standard deviation around 10%. The stoichiometric ratio between Ag and Ge precisely control the inward diffusion pathway, which means regardless of its heterogeneous deposition rate, as long as the Ag template is completely oxidized, the galvanic replacement reaction would stop immediately due to the lack of any reducing agents present in the solution. This mechanism bypasses the classic nucleation–growth synthesis route but employs Ag NPs as both reducing agent and nucleation sites. Thus, the reaction can be confined within single nanoparticle range which shows a great potential in future scale-up and industrial applications. The size of the resulting nanoparticles is solely depending on the initial size of the single metal NP and the reaction stoichiometric relationship.

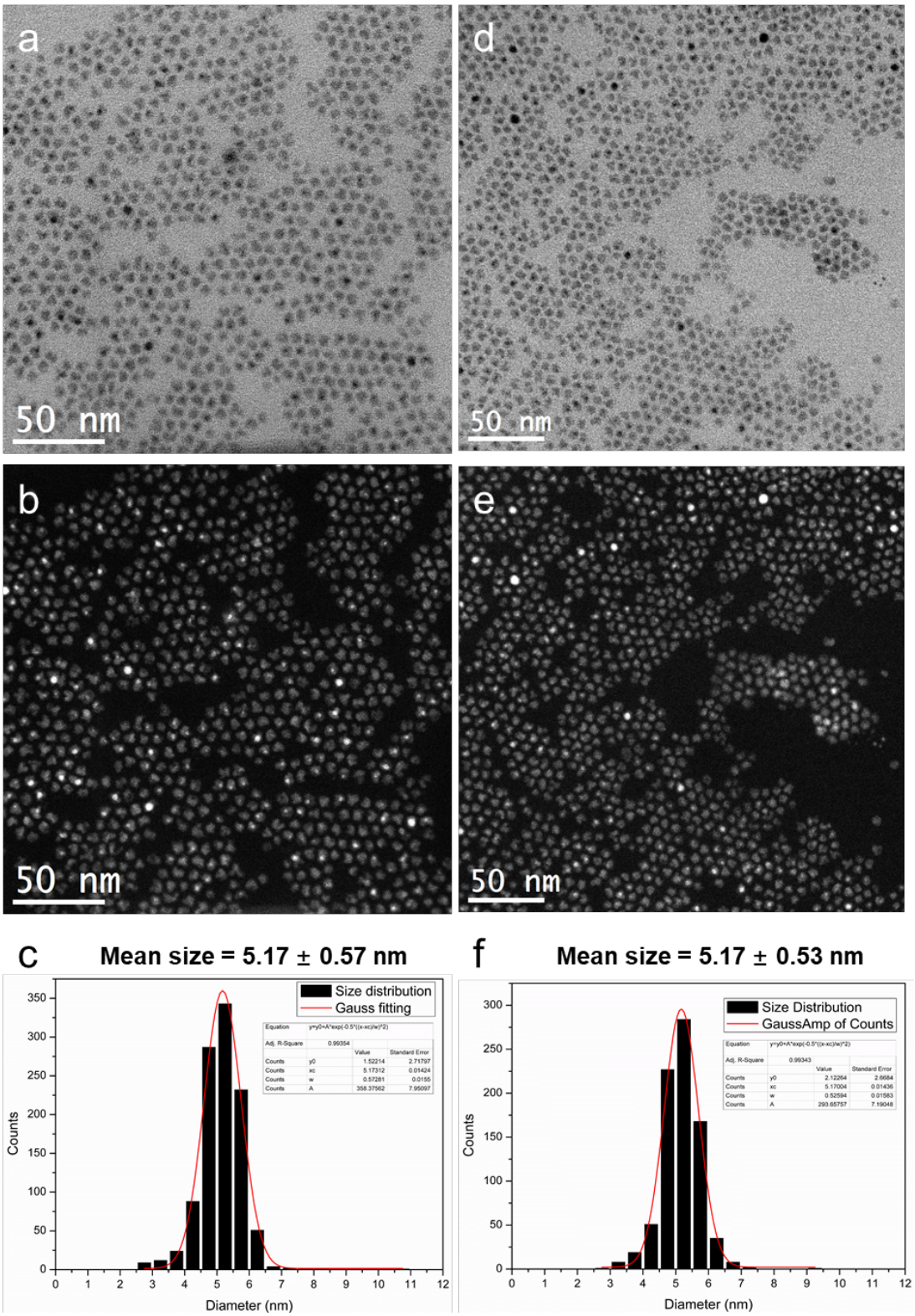

Figure 6. (a-c) BF-STEM and DF-STEM images of the sample prepared from Ag/GeI_2 = 0.3, the histogram shows a mean size of 5.17 nm ± 0.57 nm. (d-f) BF-STEM and DF-STEM images of the same sample but from different observing area.

The histogram shows a mean size of 5.17 ± 0.53 nm.

While the galvanic replacement reaction between the noble metal such as Au, Ag, Pt has been studied extensively, there is a contradictory observation of the reaction dynamic via galvanic replacement reaction from different groups. For example, most of the studies agreed with the alloying and dealloying process, and the resulting NPs possess a hollow interior with smooth surface,[16, 19, 35-37] however, some groups report a number of different observations suggesting different mechanisms, especially when the galvanic replacement was performed under organic environment.[22, 23] For example, Yang et al[38], pointed out that they observed a significant shrinkage of the Ag templates during the reaction instead of enlargement in size; they also determined that under certain conditions, the Au or Pt atoms deposited on the surface of the Ag NPs, resulting in a core-shell Ag@Au or Ag@Pt structure without the alloying and dealloying process. Our study suggests that this inconsistency may arise from a slight difference of their synthetic conditions, especially the molar ratio between the starting materials. It shows the importance of understanding the role of each component and their contribution to the structure evolution which in turn will certainly help to increase the reproducibility and future applications.

3.2.4 Temperature influence

While our studies were mainly performed at 200°C employing microwave synthesis to make the reaction external conditions consistent, the results, however, clearly show that the reaction is both thermodynamically and kinetically controlled. Thus, the study of the heating profile on the reaction is important. Based on the results described above, we can suggest that lower energy will favor the Ag@Ge core-shell formation pathway while higher energy will favor the hollowing-out pathway. While keeping all other parameters within an optimal range, a series of study were performed under different temperature settings. The results are in good agreement with our expectation. As shown in Figure 7a-c, the reaction was barely initiated at lower temperature. After 30min heating at 50°C, Figure 7a shows mainly unreacted Ag NPs; when the temperature is increased to 70°C, the products show some etching effect of the Ag template but still no well-defined hollow Ge NPs, as shown in Figure 7b. However, when the temperature is further increased to 100°C, within 30 min, the STEM image in Figure 7c shows a combination of silver NPs, solid Ge NPs, and hollow Ge NPs. This indicates the temperature has reached the necessary activation energy to trigger the hollowing-out pathway but not high enough to avoid the Ag@Ge core-shell formation. For comparison purposes, the reaction was performed at 200 °C again to test the robustness of the synthetic conditions. From Figure 7d the STEM image indicates an exclusively cubic-like hollow Ge NPs, which means under such temperature, the dissolution rate of the Ag core is high enough that the reaction follows only the hollowing-out pathway and results in only hollow Ge NPs.

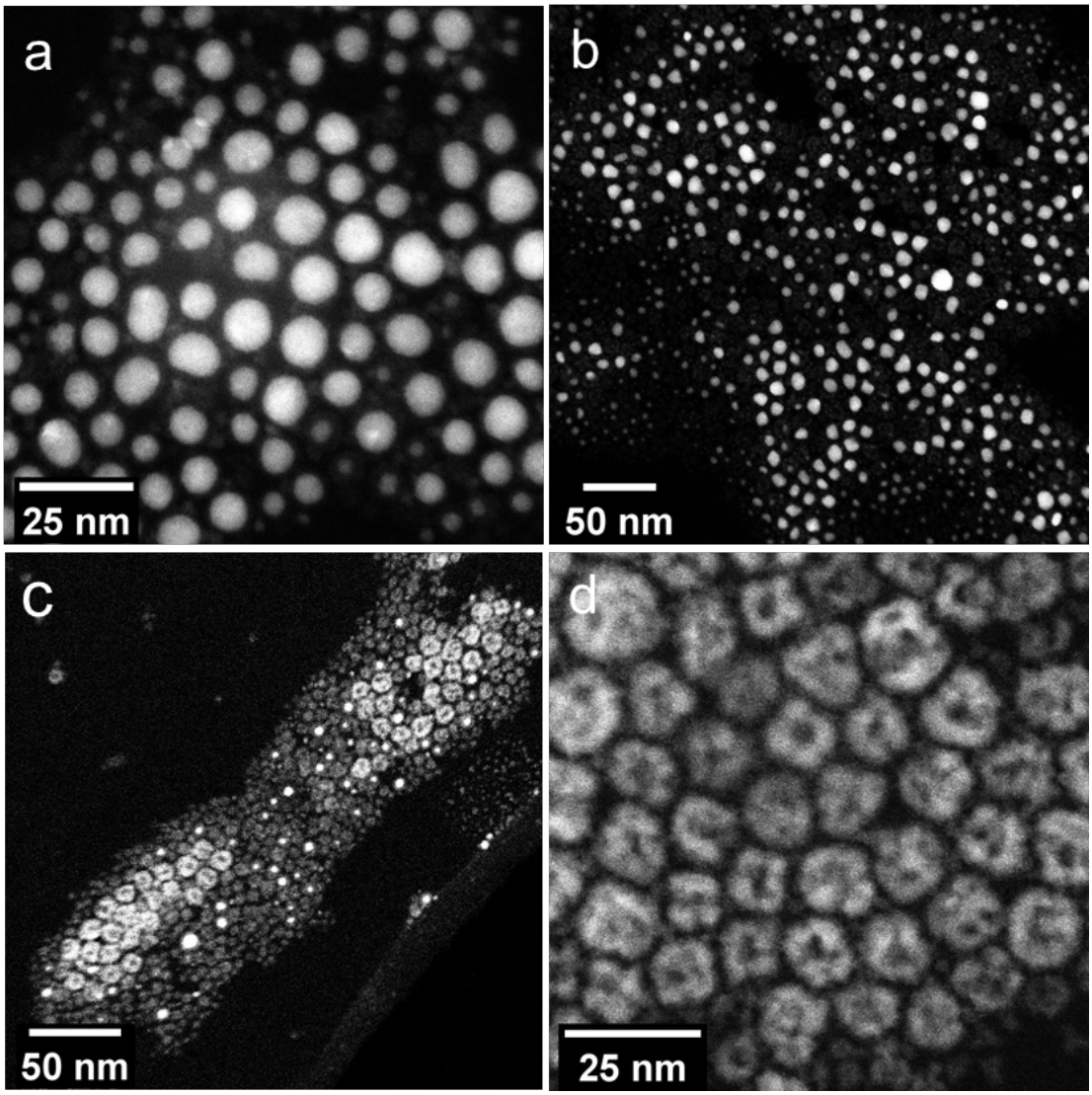

Figure 7. (a-c) HAADF-STEM image of the products from galvanic replacement reaction between GeI_2 and Ag NPs under different temperature: (a) 50 °C, (b) 70 °C, (c) 100 °C, (d) 200 °C. It shows (a) at 50 °C, the Ag template barely reacted with Ge precursor and remains intact with slightly change of its original size. (b) When the temperature rises to 70 °C, a combination of Ag@Ge core-shell structure and solid Ge NPs were synthesized. No evidence of hollow Ge NP under this condition. (c) Further increasing the temperature to 100 °C generates both hollow and solid Ge NPs and a small amount of Ag@Ge core-shell structure which indicated by the much brighter spot. (d) exclusively cubic-like hollow Ge structures via galvanic replacement at 200 °C with an optimized synthesis condition.

3.2.5 Fine-control over core-shell structure

The change of the nucleation kinetics can be used to effectively control the size and shapes

of the NPs. Especially, controlling of the thickness of the Ag@Ge core-shell structure would be desirable because it not only represents a novel route toward a metal-semiconductor core/shell NPs with larger lattice mismatch but also offer further support to the inward growth mechanism. Core-shell nanostructure via galvanic replacement was rarely reported in literature as the reactions usually possess a very low energy barrier thus could occur instantaneously even at a temperature approaching 0°C.[39-43] This type of galvanic replacement reaction is usually too favorable to be controlled thus leads to the almost inevitable formation of hollow structure. To avoid the formation of a pinhole, many synthetic strategies have been reported to prohibit the fast hollowing-out process, such as change the metal precursor or introduce a competitive reducing agent.[44-47]

In our case, however, the high energy barrier of the galvanic replacement reaction between Ag and GeI_2 indicates that we can prevent the fast hollowing-out process by simply control the temperature. In order to achieve a uniform Ag/Ge core-shell structure, we employ the same reaction conditions as before but lower the temperature in order to avoid the hollowing-out pathway. Once the reaction reaches its targeted temperature, by taking aliquots after 5 min, 15 min and 30 min of the reaction time and directly injecting into a cold methanol solution to quench the reaction, the Ag@Ge core-shell structure is successfully synthesized with different Ag core size and amorphous Ge shell thickness demonstrating that the inward replacement pathway is highly controllable. As shown in Figure 8a, after 5 min of reaction, a thin layer of amorphous Ge is coated on the Ag NP surface. The HAADF-STEM image shows the thickness of Ge shell is around 0.95 nm and the Ag core has a diameter of 8.85 nm. After 15 min of reaction, as shown in Figure 8b, the Ge shell thickness increased to around 1.2 nm and the Ag core shrinks to around 7.31 nm. Further extending the reaction to 30 min results in a Ge shell thickness of 1.51 nm and the Ag core further shrinking to 6.34 nm (Figure 8c). As we discussed above, due to the stoichiometric relationship between Ag and Ge^{2+}, for a specific amount of time, more Ag will be removed from the core with less Ge diffusing inward and the overall size of the particle will shrink. The product shown in Figure 8c was re-dispersed in toluene and a UV-vis spectrum was obtained (Figure 8d) to test its air stability and further confirm the uniformity of core-shell structure. The spectrum of the as-prepared Ag/Ge core-shell NPs show no surface plasmon peak from Ag that is expected around 421 nm and provides a typical semiconductor spectrum which in agreement with the Ag@Ge core-shell structure. By exposing the solution to air and subsequence oxidation and dissolution of the Ge shell, the absorbance around 421 nm emerges, and after 48 h of exposure, the resulting solution gives a very similar absorption curve as expected for spherical Ag NPs. This experiment shows that the amorphous Ge was covering the Ag core evenly and completely. The reaction temperature controls the kinetics of the reaction and fine-control of the core-shell thickness could be achieved by quenching the reaction at different times. Figure 9a shows the uniform Ag@Ge core-shell NPs and EDS mapping. Considering the significant lattice mismatch between Ag and Ge (38.7%), many other novel core-shell nanostructures with

controllable thickness could potentially been synthesized by applying the same strategy.

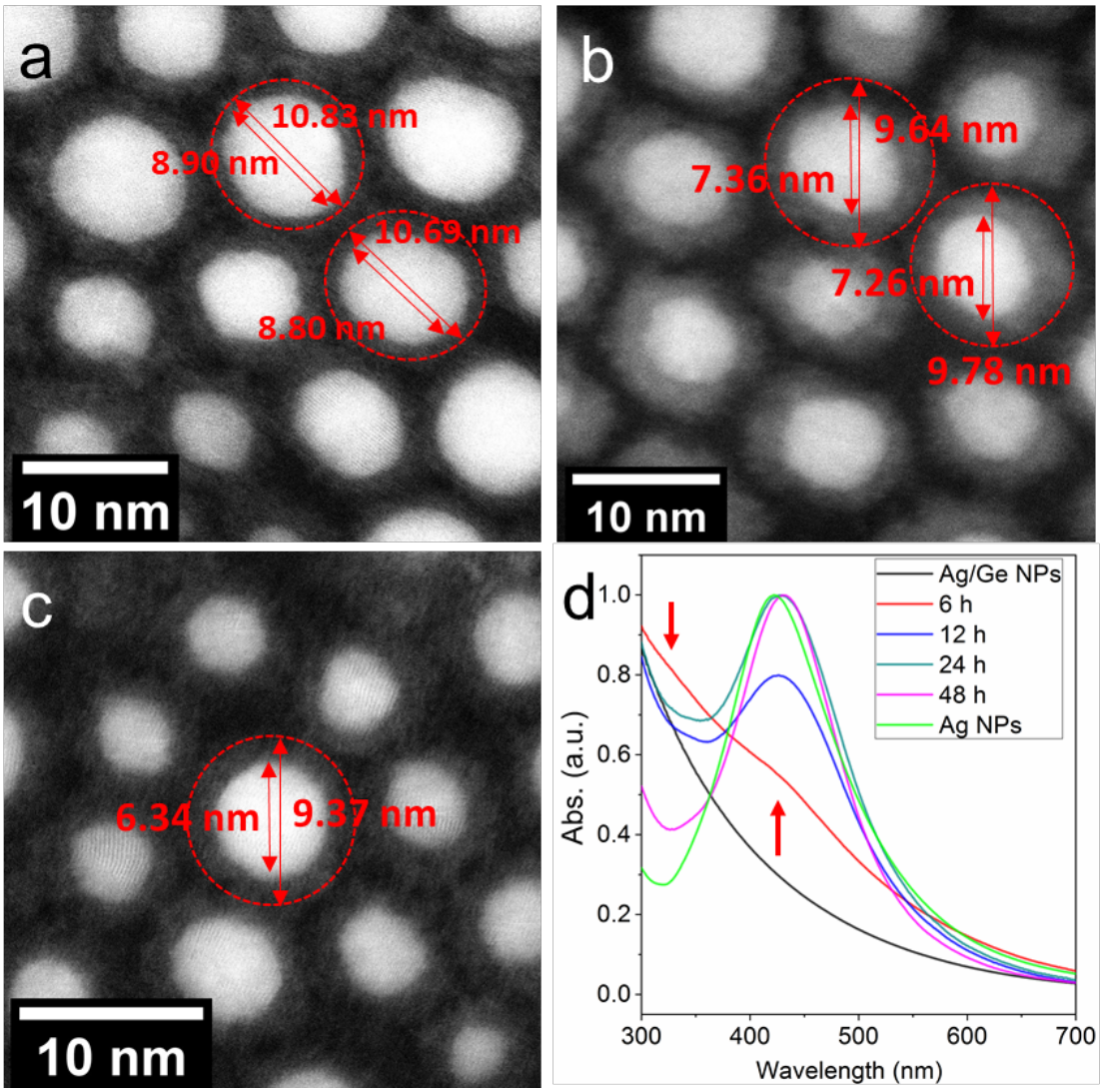

Figure 8. (a, b, c) High-angle annular dark-field (HAADF) STEM image of Ag/Ge core-shell NPs from aliquots of the reaction taken at different times: (a) 5 min, (b) 15 min, (c) 30 min. Average Ge shell thickness of samples in (a)-(c) is estimated at 0.95 nm, 1.20 nm and 1.51 nm, respectively. (d) UV-Vis spectrum of as-synthesized Ag/Ge core-shell NPs in toluene and after exposure to air over a period of 48 h. A typical UV-Vis spectrum of the starting Ag NPs in toluene is also shown in green color.

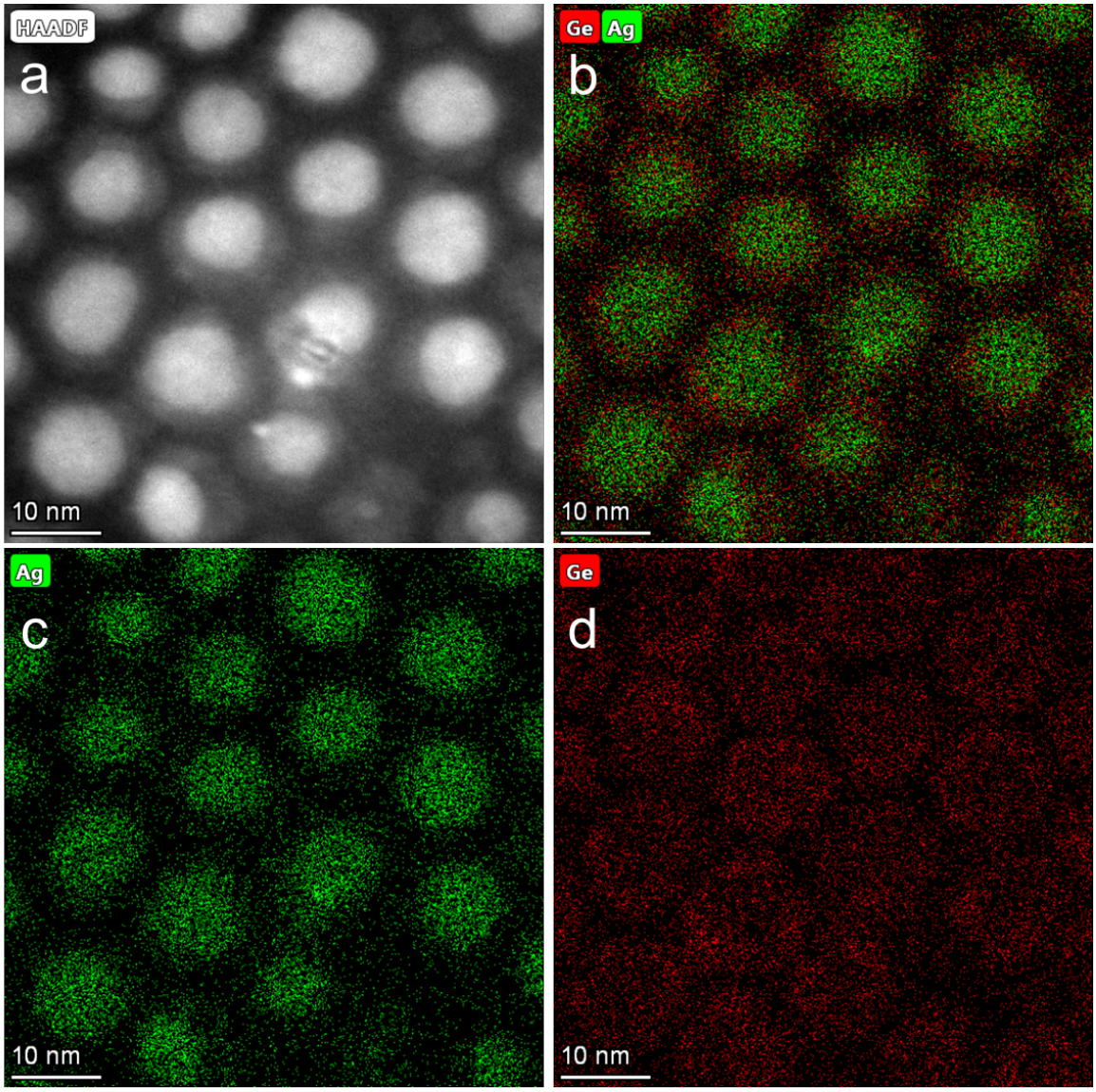

Figure 9. (a) HAADF-STEM image of Ag/Ge core-shell NPs by quench the reaction at 15min. (b-d) Combined EDS mapping from the region of (a). EDS signal shown in green comes from Ag (c) and Ge shell is shown in red (d).

4. Conclusion

We have carried out systematic studies and identified the specific roles of each reagent in the galvanic replacement reaction between GeI_2 and silver nanoparticles. We have also explored the influence of different synthetic parameters such as temperature and reaction time on the reaction. The results are summarized in Figure 10:

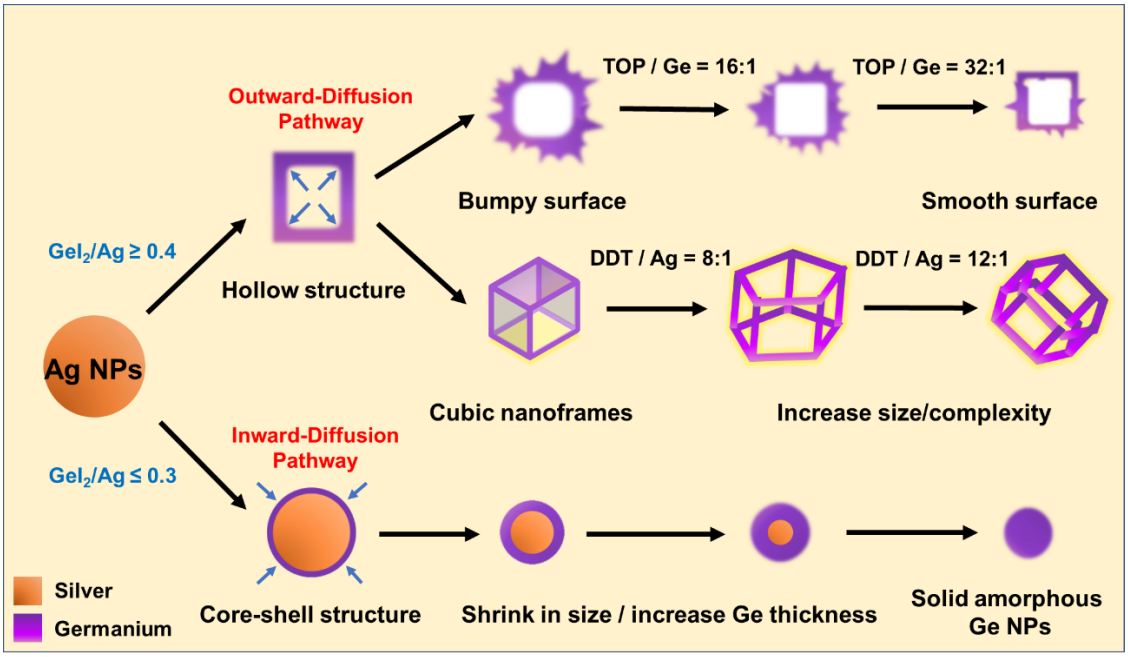

Figure 10. Schematic illustration summarizing competitive two different diffusion pathway and structural changes involved in the galvanic replacement reaction between a polycrystalline silver nanoparticle and GeI_2. The binding ligand TOP and DDT can also induce a morphological change on the final Ge NPs.

Our systematic study reveals the specific roles of important ligands including TOP and DDT in the galvanic replacement reaction between GeI_2 and Ag NPs. TOP is serving as a stabilizing agent of the inorganic GeI_2 precursor to make it easily dissolved in nonaqueous solution which ensure the effective contacting between Ag template and Ge^{2+} ions. Higher concentration of TOP would lead to a much smoother surface of the hollow Ge NPs while lower TOP content would result in hollow Ge NPs with more dangling bonds and bumpy surface. DDT, on the other hand, was found to be critical to the geometry evolution of the hollow Ge NPs. With a higher concentration of DDT, more vacancies will be generated on the surface of the particles, leading to the formation of larger and more complex hollow Ge NPs with multiple porous walls.

In addition, the initial molar ratio between Ag NPs and GeI_2 shows a key role in determining the morphology and composition of the final products. On the Ge-deficient range, the formation of hollow structure can be prohibited even under high temperature (e.g. 200°C). When the concentration of Ge precursor is efficiently lower than the 0.5 Ge/Ag stoichiometric molar ratio (e.g. Ge/Ag = 0.3), the Ag-Ge diffusion rate could be significantly decreased and follow the inward diffusion pathway which leading to the formation of pure solid Ge NPs with reduced size compare to the Ag templates. On the other hand, only higher germanium precursor presents in the synthesis (e.g. Ge/Ag > 0.4) will lead to the formation of hollow nanostructure. The colloidal Ge NPs are stable under

noble gas condition. When the nanoparticles were suspended in anhydrous toluene and stored in an Argon filled glovebox, the morphology of the hollow Ge NPs and the Ag/Ge domains in the core-shell NPs can be maintained without any changes even after one year.

To the best of our knowledge, our study demonstrates the first successful synthesis of metal-semiconductor core-shell structure with a controllable core and shell thickness via galvanic replacement alone, considering the huge lattice mismatch between Ag and Ge (38.7%). The core/shell thickness ratio could be controlled by selectively quenching the reaction at different stages. With a reasonable temperature range, the galvanic replacement reaction can be controlled to follow only core-shell growth pathway or fast hollowing-out pathway. This result shows that galvanic replacement reaction can serve as a really powerful tool to generate novel structure due to its versatile mechanism and flexibility.

Collectively, our study reveals the multiple aspects of the galvanic replacement reaction between Ag and GeI_2. The reaction can follow the outward fast hollowing-out pathway or inward core-shell pathway depends on the synthesis condition. We also disclose the specific role of each binding ligand in the reaction, which can serve as a guild to design other galvanic replacement reaction in nonaqueous environment. What's more, we report the successful synthesis of highly monodisperse solid amorphous Ge NPs follow the inward growth mechanism, for the first time. The unique mechanism allows the reaction to be self-terminated and achieve nanometer-sized accuracy. The galvanic reaction may be applied to other semiconductors and could serve as a powerful alternative to the classic nucleation-growth mechanism and subsequently advance the scale up and further applications.

Associated content

Supporting information

Synthesis details of all reactions for the systematic study, EDS spectrum of hollow Ge NPs and HAADF-STEM images of irregular Ge NPs and agglomerated Ag NPs.

Author information

Corresponding Author

*E-mail: smkauzlarich@ucdavis.edu

ORCID
Xiao Qi: 0000-0003-4884-6454

Susan M. Kauzlarich: 0000-0002-3627-237X

Notes
The authors declare no competing financial interest.

Acknowledgements
This work was supported by the National Science Foundation CHE- 1710110. Electron microscopy at the Molecular Foundry was supported by the Office of Science, Office of Basic Energy Sciences, of the U.S. Department of Energy under Contract No. DE-AC02-05CH11231. We thank Dr. Karen Bustillo at National Center for Electron Microcopy at Lawrence Berkeley National Laboratory and Dr. Andrew Thron at Advanced Materials Characterization and Testing Laboratory (AMCaT) at UC Davis for their help with TEM and STEM measurements and all useful discussions.

References

1. Aricò, A. S.; Bruce, P.; Scrosati, B.; Tarascon, J.-M.; van Schalkwijk, W., Nanostructured materials for advanced energy conversion and storage devices. *Nature Materials* **2005,** *4* (5), 366-377.
2. Choi, S.; Kim, J.; Choi, N.-S.; Kim, M. G.; Park, S., Cost-Effective Scalable Synthesis of Mesoporous Germanium Particles via a Redox-Transmetalation Reaction for High-Performance Energy Storage Devices. *ACS Nano* **2015,** *9* (2), 2203-2212.
3. Son, I. H.; Park, J. H.; Park, S.; Park, K.; Han, S.; Shin, J.; Doo, S.-G.; Hwang, Y.; Chang, H.; Choi, J. W., Graphene balls for lithium rechargeable batteries with fast charging and high volumetric energy densities. *Nature Communications* **2017,** *8* (1), 1561.
4. Lu, J.; Wu, T.; Amine, K., State-of-the-art characterization techniques for advanced lithium-ion batteries. *Nature Energy* **2017,** *2* (3), 17011.
5. An, Y.; Fei, H.; Zeng, G.; Xu, X.; Ci, L.; Xi, B.; Xiong, S.; Feng, J.; Qian, Y., Vacuum distillation derived 3D porous current collector for stable lithium–metal batteries. *Nano Energy* **2018,** *47*, 503-511.
6. Tarascon, J. M.; Armand, M., Issues and challenges facing rechargeable lithium batteries. *Nature* **2001,** *414* (6861), 359-367.
7. Park, M.-H.; Cho, Y.; Kim, K.; Kim, J.; Liu, M.; Cho, J., Germanium Nanotubes Prepared by Using the Kirkendall Effect as Anodes for High-Rate Lithium Batteries. *Angewandte Chemie International Edition* **2011,** *50* (41), 9647-9650.
8. Li, W.; Li, M.; Yang, Z.; Xu, J.; Zhong, X.; Wang, J.; Zeng, L.; Liu, X.; Jiang, Y.; Wei, X.; Gu, L.; Yu, Y., Carbon-Coated Germanium Nanowires on Carbon Nanofibers as Self-Supported Electrodes for Flexible Lithium-Ion Batteries. *Small* **2015,** *11* (23), 2762-2767.
9. Wu, S.; Han, C.; Iocozzia, J.; Lu, M.; Ge, R.; Xu, R.; Lin, Z., Germanium-Based

Nanomaterials for Rechargeable Batteries. *Angew Chem Int Ed Engl* **2016,** *55* (28), 7898-7922.
10. Vaughn Ii, D. D.; Schaak, R. E., Synthesis, properties and applications of colloidal germanium and germanium-based nanomaterials. *Chemical Society Reviews* **2013,** *42* (7), 2861-2879.
11. He, R.; Sazio, P. J. A.; Peacock, A. C.; Healy, N.; Sparks, J. R.; Krishnamurthi, M.; Gopalan, V.; Badding, J. V., Integration of gigahertz-bandwidth semiconductor devices inside microstructured optical fibres. *Nature Photonics* **2012,** *6*, 174.
12. Gärtner, K.; Jöhrens, J.; Steinbach, T.; Schnohr, C. S.; Ridgway, M. C.; Wesch, W., Void formation in amorphous germanium due to high electronic energy deposition. *Physical Review B* **2011,** *83* (22), 224106.
13. Sayed, S. Y.; Buriak, J. M., Epitaxial Growth of Nanostructured Gold Films on Germanium via Galvanic Displacement. *ACS Applied Materials & Interfaces* **2010,** *2* (12), 3515-3524.
14. Oh, M. H.; Yu, T.; Yu, S.-H.; Lim, B.; Ko, K.-T.; Willinger, M.-G.; Seo, D.-H.; Kim, B. H.; Cho, M. G.; Park, J.-H.; Kang, K.; Sung, Y.-E.; Pinna, N.; Hyeon, T., Galvanic Replacement Reactions in Metal Oxide Nanocrystals. *Science* **2013,** *340* (6135), 964.
15. El Mel, A.-A.; Chettab, M.; Gautron, E.; Chauvin, A.; Humbert, B.; Mevellec, J.-Y.; Delacote, C.; Thiry, D.; Stephant, N.; Ding, J.; Du, K.; Choi, C.-H.; Tessier, P.-Y., Galvanic Replacement Reaction: A Route to Highly Ordered Bimetallic Nanotubes. *The Journal of Physical Chemistry C* **2016,** *120* (31), 17652-17659.
16. Xia, X.; Wang, Y.; Ruditskiy, A.; Xia, Y., 25th Anniversary Article: Galvanic Replacement: A Simple and Versatile Route to Hollow Nanostructures with Tunable and Well-Controlled Properties. *Advanced Materials* **2013,** *25* (44), 6313-6333.
17. González, E.; Arbiol, J.; Puntes, V. F., Carving at the Nanoscale: Sequential Galvanic Exchange and Kirkendall Growth at Room Temperature. *Science* **2011,** *334* (6061), 1377.
18. Sun, Y.; Xia, Y., Shape-Controlled Synthesis of Gold and Silver Nanoparticles. *Science* **2002,** *298* (5601), 2176.
19. Sun, Y.; Xia, Y., Mechanistic Study on the Replacement Reaction between Silver Nanostructures and Chloroauric Acid in Aqueous Medium. *Journal of the American Chemical Society* **2004,** *126* (12), 3892-3901.
20. Lin, Z.-W.; Tsao, Y.-C.; Yang, M.-Y.; Huang, M. H., Seed-Mediated Growth of Silver Nanocubes in Aqueous Solution with Tunable Size and Their Conversion to Au Nanocages with Efficient Photothermal Property. *Chemistry* **2016,** *22* (7), 2326-2332.
21. Wu, Y.; Sun, X.; Yang, Y.; Li, J.; Zhang, Y.; Qin, D., Enriching Silver Nanocrystals with a Second Noble Metal. *Accounts of Chemical Research* **2017,** *50* (7), 1774-1784.
22. Yang, J.; Lee, J. Y.; Ying, J. Y., Phase transfer and its applications in nanotechnology. *Chemical Society Reviews* **2011,** *40* (3), 1672-1696.
23. Yang, J.; Lee, J. Y.; Too, H.-P., Core−Shell Ag−Au Nanoparticles from Replacement Reaction in Organic Medium. *The Journal of Physical Chemistry B* **2005,** *109* (41), 19208-19212.
24. Nolan, B. M.; Chan, E. K.; Zhang, X.; Muthuswamy, E.; van Benthem, K.; Kauzlarich, S. M., Sacrificial Silver Nanoparticles: Reducing GeI2 To Form Hollow Germanium Nanoparticles by Electroless Deposition. *ACS Nano* **2016,** *10* (5), 5391-5397.
25. Hiramatsu, H.; Osterloh, F. E., A Simple Large-Scale Synthesis of Nearly Monodisperse Gold

and Silver Nanoparticles with Adjustable Sizes and with Exchangeable Surfactants. *Chemistry of Materials* **2004,** *16* (13), 2509-2511.
26. Peng, S.; McMahon, J. M.; Schatz, G. C.; Gray, S. K.; Sun, Y., Reversing the size-dependence of surface plasmon resonances. *Proceedings of the National Academy of Sciences* **2010,** *107* (33), 14530-14534.
27. Sun, Y., Controlled synthesis of colloidal silver nanoparticles in organic solutions: empirical rules for nucleation engineering. *Chemical Society Reviews* **2013,** *42* (7), 2497-2511.
28. Chen, J.; Wiley, B.; McLellan, J.; Xiong, Y.; Li, Z.-Y.; Xia, Y., Optical Properties of Pd−Ag and Pt−Ag Nanoboxes Synthesized via Galvanic Replacement Reactions. *Nano Letters* **2005,** *5* (10), 2058-2062.
29. He, J.; Kanjanaboos, P.; Frazer, N. L.; Weis, A.; Lin, X.-M.; Jaeger Heinrich, M., Fabrication and Mechanical Properties of Large-Scale Freestanding Nanoparticle Membranes. *Small* **2010,** *6* (13), 1449-1456.
30. Lu, X.; Au, L.; McLellan, J.; Li, Z.-Y.; Marquez, M.; Xia, Y., Fabrication of Cubic Nanocages and Nanoframes by Dealloying Au/Ag Alloy Nanoboxes with an Aqueous Etchant Based on Fe(NO3)3 or NH4OH. *Nano Letters* **2007,** *7* (6), 1764-1769.
31. Zeng, J.; Zhang, Q.; Chen, J.; Xia, Y., A Comparison Study of the Catalytic Properties of Au-Based Nanocages, Nanoboxes, and Nanoparticles. *Nano Letters* **2010,** *10* (1), 30-35.
32. Au, L.; Lu, X.; Xia, Y., A Comparative Study of Galvanic Replacement Reactions Involving Ag Nanocubes and AuCl2− or AuCl4−. *Advanced Materials* **2008,** *20* (13), 2517-2522.
33. Wang, W.; Dahl, M.; Yin, Y., Hollow Nanocrystals through the Nanoscale Kirkendall Effect. *Chemistry of Materials* **2013,** *25* (8), 1179-1189.
34. Tang, Y.; Ouyang, M., Tailoring properties and functionalities of metal nanoparticles through crystallinity engineering. *Nature Materials* **2007,** *6*, 754.
35. Sun, Y.; Mayers, B. T.; Xia, Y., Template-Engaged Replacement Reaction: A One-Step Approach to the Large-Scale Synthesis of Metal Nanostructures with Hollow Interiors. *Nano Letters* **2002,** *2* (5), 481-485.
36. Sun, Y.; Xia, Y., Multiple-Walled Nanotubes Made of Metals. *Advanced Materials* **2004,** *16* (3), 264-268.
37. Tan, S. F.; Lin, G.; Bosman, M.; Mirsaidov, U.; Nijhuis, C. A., Real-Time Dynamics of Galvanic Replacement Reactions of Silver Nanocubes and Au Studied by Liquid-Cell Transmission Electron Microscopy. *ACS Nano* **2016,** *10* (8), 7689-7695.
38. Yang, J.; Yang Lee, J.; Too, H.-P., Phase-Transfer Identification of Core-Shell Structures in Bimetallic Nanoparticles. *Plasmonics* **2006,** *1* (1), 67-78.
39. Sun, Y.; Mayers, B.; Xia, Y., Metal Nanostructures with Hollow Interiors. *Advanced Materials* **2003,** *15* (7‐8), 641-646.
40. Skrabalak, S. E.; Au, L.; Li, X.; Xia, Y., Facile synthesis of Ag nanocubes and Au nanocages. *Nature Protocols* **2007,** *2*, 2182.
41. Seo, D.; Song, H., Asymmetric Hollow Nanorod Formation through a Partial Galvanic Replacement Reaction. *Journal of the American Chemical Society* **2009,** *131* (51), 18210-18211.
42. McEachran, M.; Keogh, D.; Pietrobon, B.; Cathcart, N.; Gourevich, I.; Coombs, N.;

Kitaev, V., Ultrathin Gold Nanoframes through Surfactant-Free Templating of Faceted Pentagonal Silver Nanoparticles. *Journal of the American Chemical Society* **2011,** *133* (21), 8066-8069.
43. Hong, X.; Wang, D.; Cai, S.; Rong, H.; Li, Y., Single-Crystalline Octahedral Au–Ag Nanoframes. *Journal of the American Chemical Society* **2012,** *134* (44), 18165-18168.
44. Gao , C.; Lu , Z.; Liu , Y.; Zhang, Q.; Chi, M.; Cheng, Q.; Yin, Y., Highly Stable Silver Nanoplates for Surface Plasmon Resonance Biosensing. *Angewandte Chemie International Edition* **2012,** *51* (23), 5629-5633.
45. Yang, Y.; Liu, J.; Fu, Z.-W.; Qin, D., Galvanic Replacement-Free Deposition of Au on Ag for Core–Shell Nanocubes with Enhanced Chemical Stability and SERS Activity. *Journal of the American Chemical Society* **2014,** *136* (23), 8153-8156.
46. Shahjamali, M. M.; Bosman, M.; Cao, S.; Huang, X.; Saadat, S.; Martinsson, E.; Aili, D.; Tay, Y. Y.; Liedberg, B.; Loo, S. C. J.; Zhang, H.; Boey, F.; Xue, C., Gold Coating of Silver Nanoprisms. *Advanced Functional Materials* **2012,** *22* (4), 849-854.
47. Sanedrin, R. G.; Georganopoulou, D. G.; Park, S.; Mirkin, C. A., Seed-Mediated Growth of Bimetallic Prisms. *Advanced Materials* **2005,** *17* (8), 1027-1031.